AD-A130 570 RAMAN STUDIES OF CUTCNQ: RESONANCE RAMAN SPECTRAL OBSERVATIONS AND CALCUL..(U) BROWN UNIV PROVIDENCE RI DEPT OF CHEMISTRY E I KAMITSOS ET AL. 07 JUL 83 1/1

UNCLASSIFIED TR-83-06 N00014-75-C-0883 F/G 7/4 NL

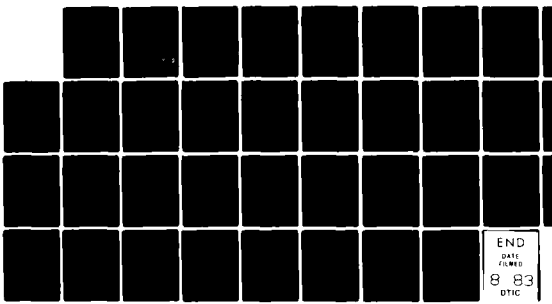

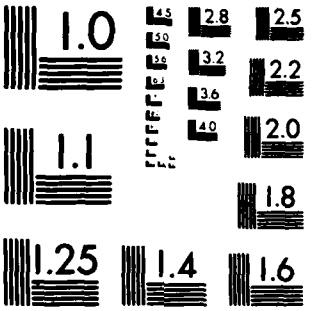

MICROCOPY RESOLUTION TEST CHART
NATIONAL BUREAU OF STANDARDS-1963-A

(11)

OFFICE OF NAVAL RESEARCH

Contract ONR-N00014-75-C-0883 NR-051-539

TECHNICAL REPORT NO. TR83-06

Raman Studies of CuTCNQ: Resonance Raman Spectral Observations and Calculations for TCNQ Ion-Radicals

by

E. I. Kamitsos and W. M. Risen, Jr.

Prepared for Publication

in

Journal of Chemical Physics

July 7, 1983

Department of Chemistry

Brown University

Providence, R.I. 02912

SECURITY CLASSIFICATION OF THIS PAGE (When Data Entered)

REPORT DOCUMENTATION PAGE		READ INSTRUCTIONS BEFORE COMPLETING FORM
1. REPORT NUMBER TR-83-06	2. GOVT ACCESSION NO. A130570	3. RECIPIENT'S CATALOG NUMBER
4. TITLE (and Subtitle) Raman Studies of CuTCNQ: Resonance Raman Spectral Observations and Calculations for TCNQ Ion-Radicals		5. TYPE OF REPORT & PERIOD COVERED Technical 6. PERFORMING ORG. REPORT NUMBER
7. AUTHOR(s) E.I. Kamitsos and W.M. Risen, Jr.		8. CONTRACT OR GRANT NUMBER(s) N00014-75-C-0883 NR-051-539
9. PERFORMING ORGANIZATION NAME AND ADDRESS Department of Chemistry Brown University Providence, Rhode Island 02912		10. PROGRAM ELEMENT, PROJECT, TASK AREA & WORK UNIT NUMBERS ONR-N00014-75-C-0883 NR-051-539
11. CONTROLLING OFFICE NAME AND ADDRESS Office of Naval Research United States Navy		12. REPORT DATE July 7, 1983 13. NUMBER OF PAGES 46
14. MONITORING AGENCY NAME & ADDRESS(if different from Controlling Office)		15. SECURITY CLASS. (of this report) 15a. DECLASSIFICATION/DOWNGRADING SCHEDULE

16. DISTRIBUTION STATEMENT (of this Report)

Distribution Unlimited; Approved for Public Release

17. DISTRIBUTION STATEMENT (of the abstract entered in Block 20, if different from Report)

18. SUPPLEMENTARY NOTES

19. KEY WORDS (Continue on reverse side if necessary and identify by block number)

charge transfer, TCNQ, CuTCNQ, Raman, Resonance Raman, Optical switching, Raman intensities, optical transformation

20. ABSTRACT (Continue on reverse side if necessary and identify by block number)

The Raman spectra of thin film, and powdered crystalline forms of CuTCNQ have been studied and analyzed in connection with their electronic spectra, and vibrational normal coordinate analysis and molecular orbital results. Non-resonance and resonance Raman conditions have been obtained by using different sample forms and source wavelengths. Shifts of $TCNQ^-$ and $TCNQ^=$ vibrational frequencies from those of $TCNQ^0$ due to changes in the charge on the TCNQ moiety have been calculated in terms of molecular orbital parameters and $TCNQ^0$ vibrational frequencies. The resonance Raman enhancement of $TCNQ^-$ in the red band system is shown to be of Franck-Condon origin and its resonance Raman spectrum in this region is calculated.

Transformation of CuTCNQ to $TCNQ^0$ with different laser lines is explained on the basis of photoinduced electronic transitions.

DD FORM 1 JAN 73 1473 EDITION OF 1 NOV 65 IS OBSOLETE
S/N 0102-014-6601

SECURITY CLASSIFICATION OF THIS PAGE (When Data Entered)

Raman Studies in CuTCNQ: Resonance Raman Spectral Observations and Calculations for TCNQ Ion-Radicals

Efstratios I. Kamitsos and William M. Risen, Jr.
Department of Chemistry
Brown University
Providence, RI 02912

Abstract

The Raman spectra of thin film, and powdered crystalline forms of CuTCNQ have been studied and analyzed in connection with their electronic spectra, and vibrational normal coordinate analysis and molecular orbital results. Non-resonance and resonance Raman conditions have been obtained by using different sample forms and source wavelengths. Shifts of $TCNQ^-$ and $TCNQ^=$ vibrational frequencies from those of $TCNQ^\circ$ due to changes in the charge on the TCNQ moiety have been calculated in terms of molecular orbital parameters and $TCNQ^\circ$ vibrational frequences. The resonance Raman enhancement of $TCNQ^-$ in the red band system is shown to be of Franck-Condon origin and its resonance Raman spectrum in this region is calculated.

Transformation of CuTCNQ to $TCNQ^\circ$ with different laser lines is explained on the basis of photoinduced electronic transitions.

Introduction

Recently we employed Raman spectroscopy to help elucidate the mechanism of the rapid electric field-induced switching of CuTCNQ films from a high- to a low impedance state (1). In the course of that study we also found that transformations of CuTCNQ to products that are spectroscopically similar to those produced electrically are induced by visible light (2,3). In fact, the use of light can make the process go beyond the electric field-induced partial transformation, which yields a material containing Cu° and TCNQ° moieties as well as untransformed CuTCNQ, as initially suggested for electric field induced switching (4), to eventually yield only Cu° and TCNQ°. The light-induced transformation proceeds without application of an electric field and is reversible. The electric field-induced transformation does not require direct contact of the material with electrodes.

In order to understand these phenomena and relate them to one another it is important to understand the effects of visible light-excitation on the system. Accordingly, we have carried out a Raman spectral study to determine the ways in which various vibrational modes interact resonantly with light in this region. We report the resonance Raman spectra of CuTCNQ obtained at selected excitation frequencies within its electronic absorption bands. Spectra ranging from non-resonance to full resonance conditions have been obtained on thin CuTCNQ films. As discussed below, particular attention is paid to resonance Raman enhancement in the red (absorption) band system ($\lambda > 550$ nm), because of the nature of the electronic transitions and the fact that optical transformation of CuTCNQ can be affected with such low energy photons. However, resonance enhancements at higher source frequencies also are reported. Since the objective is to develop our understanding of these systems, attempts to relate reported electronic structures (5-7) and vibrational analyses (8-11) to both the vibrational

shifts occurring upon charge transfer and the resonance enhancements occurring upon visible excitation are reported. In the latter case the relative intensities of resonantly enhanced modes have been calculated approximately using a scattering tensor of Franck-Condon origin.

Vibrational spectroscopy has proven to be quite useful for studying charge transfer compounds generally, since their charge distributions can often be probed by monitoring vibrational frequency shifts. In TCNQ-based systems, this is well illustrated by the identification of both neutral and negatively charged TCNQ-units in $Cs_2(TCNQ)_3$ by Raman and infrared spectroscopy (12). In addition, a measure of the degree of charge-transfer between donor- and acceptor-molecules, which is essential to understanding the conduction mechanism in charge-transfer salts (13), has been obtained in many cases from their Raman frequencies. This has been done by employing a linear relationship between vibrational frequency and charge density that was established on systems whose average charge per molecule can be determined stoichiometrically (14,15). The vibrational spectra of TCNQ derivatives are particularly sensitive to the charge on the TCNQ moiety. The observed shifts in vibrational frequency that occur as the TCNQ charge is varied have been correlated qualitatively with bond order-changes that occur upon ionization. In this work we also show that such shifts, especially those of the totally symmetric modes, can be calculated quantitatively reasonably well by using reported vibrational analyses and molecular orbital calculations on TCNQ and $TCNQ^-$.

As mentioned briefly above, we have observed that CuTCNQ (as well as AgTCNQ) can be transformed by light at powers above certain limits either partially or completely to Cu° and $TCNQ^\circ$. The nature and extent of this reversible phenomenon is discussed in light of the optical excitations and resonance Raman results.

Experimental

The TCNQ (7,7,8,8-tetracyanoquinodimethane) used was purchased from Aldrich Chemical Co., recrystallized from dry acetonitrile (CH_3CN) and then sublimed *in vacuo* on to a PTFE (teflon) surface. The CuTCNQ was prepared for spectral study by three methods. Pure CuTCNQ salt was synthesized, following the method of Melby, *et al* (16), by mixing warm CH_3CN solutions of CuI and TCNQ in a 3:2 mole ratio to prevent oxidation of CuTCNQ by I_2(1), separating the dark blue CuTCNQ precipitate by filtration, washing it with dry CH_3CN and finally washing it with a large volume of dry diethyl ether. In the second method, polycrystalline CuTCNQ films of *ca* 5 μm thickness were prepared on Cu foils, which had been cleaned mechanically and then chemically in 1.5 M H_2SO_4, by dipping the dry foils into a CH_3CN solution of TCNQ. This employs the well known fact that TCNQ solutions react with metallic Cu (or Ag) at 25°C to form the metal salts of $TCNQ^-$ (16), and produce deep blue CuTCNQ films on the Cu substrate in a few minutes. Such Cu/CuTCNQ films were washed with CH_3CN and then dried *in vacuo*.

In the third method, thin CuTCNQ films were prepared on a variety of substrates (fused silica, Cu, Al, KBr) by a vapor deposition technique. First Cu metal was vapor deposited on the substrate, and, without breaking the vacuum, the stoichiometrically appropriate amount of TCNQ to achieve a 1:1 mole ratio was deposited. If thicker films are needed, alternating Cu and TCNQ layers are deposited. Since Raman spectra of as-deposited film structures showed that TCNQ had not reacted under the deposition conditions, they were heated at *ca* 100°C for a few minutes *in vacuo* or under Ar. The resultant films are light blue-green, smooth and apparently homogeneous, and gave the characteristic CuTCNQ Raman spectrum with no bands for $TCNQ^\circ$. Infrared (transmission or reflectance) and Raman measurements showed that all three methods produce the

$Cu^{+}TCNQ^{-}$ (1,2).

The visible spectra of the different forms of CuTCNQ were measured on a Cary Model 17 spectrometer. The Raman spectra were obtained on a Jarrell-Ash 25-300 spectrometer using a 90° scattering geometry. The excitation was provided by lines of an Ar ion laser (Spectra Physics 165) and He-Ne laser (Spectra Physics 125). The spectral accuracy and resolution was 2 cm^{-1}. Since the light-induced transformations of stationary CuTCNQ samples were observed in the initial stages of the work when the Raman source power exceeded certain threshold values (2,3), spinning sample techniques and careful control of source power were employed to measure the spectra of the untransformed CuTCNQ samples.

Results

The visible spectra and the resonance Raman spectra of the several forms of CuTCNQ were obtained as described above and are presented and analyzed in the following sections. It will be helpful in presenting the Raman results to have considered the visible spectra first.

Visible Absorption Spectra

The optical absorption spectra of charge-transfer compounds of TCNQ are related closely both to their resonance Raman spectra and to the remarkable electrical properties they exhibit (17). In Fig. 1 the electronic absorption spectra of CuTCNQ in three different physical forms are shown. That of a CH_3CN solution of CuTCNQ is shown in Fig. 1a, that of a CuTCNQ thin film (< 0.5 μm) formed by the evaporation-heating technique on a fused silica plate is shown in Fig. 1b, and the spectrum of a nujol mull of CuTCNQ salt prepared from CuI is in Fig. 1c. The three spectra are quite different. Clearly the spectrum of the thin film represents an intermediate situation between those shown

in Figs. 1a and 1c.

The spectrum of CuTCNQ in solution is identical to that of LiTCNQ (18), KTCNQ (19,20) and electrogenerated $TCNQ^{\cdot-}$ (21). It is characterized by four major bands which appear at ca 843, 743, 680 and 415 nm. The strongest peaks are at 420 and 843 nm and occur with an intensity ratio of ca 0.5, which is typical of simple $TCNQ^-$ salts (16).

The π-electron system of $TCNQ^-$ has been studied theoretically. Lowitz (5) reported a semiempirical SCF-LCAO-MO treatment initially, and subsequently others have reported SCF-MO (PP and MN) (6) and CNDO/S-CI (7) treatments. While these studies are not in complete agreement, generally the red band system (550-900 nm) is assigned to the $^2B_{2g} \rightarrow {}^2B_{1u}^{(1)}$ (long axis polarized) and the blue band system (350-500 nm) is assigned to overlapping $^2B_{2g} \rightarrow {}^2B_{1u}^{(2)}$ (long axis polarized) and $^2B_{2g} \rightarrow {}^2A_u$ (short axis polarized) transitions.

The spectra of a variety of solid TCNQ anion-radical salts have been studied (17,19,22-25), and the electronic transitions have been grouped into three types (17,19,25). The intramolecular (or locally excited) transitions are denoted LE, with the lower energy one LE_1 and the higher LE_2, while the intermolecular charge-transfer transitions are classified as CT_1 for charge-transfer between two $TCNQ^-$ ions and CT_2 for that between a $TCNQ^-$ anion and neutral TCNQ°.

Salts with a 1:1 mole ratio of cation to TCNQ and complete charge-transfer from donor to TCNQ (ρ=1), show the LE_1, LE_2 and CT_1 bands. The position of the CT_1 band, at the high energy side of the near infrared spectrum, is correlated to the electrical properties of these salts (17,19,24). In the cases of LiTCNQ, NaTCNQ, and KTCNQ, for example, CT_1 is found at 1280, 1075 and 1180 nm (19), respectively, and the salts have parallel conductivities of 5×10^{-5}, 1×10^{-5} 1×10^{-4} Ω^{-1} cm^{-1} (26). It is important to note that other determinants of geometry, such as cation size, also affect the exact position of CT_1. In 1:1

charge transfer salts high electrical conductivity can result from incomplete charge transfer, as it does in the case of TTF-TCNQ which has a room temperature conductivity $\sigma \approx 10^3 \Omega^{-1}$ cm^{-1} (27), a degree of charge transfer $\rho = 0.59$ (28), and bands at ca 11.0 kK (CT_1) and 2.8 kK (CT_2) (29). Complex TCNQ salts with 1:2 or 2:3 mole ratios containing both neutral and monoanionic TCNQ-moieties, have intermediate conductivities, and their spectra exhibit both CT_1 and CT_2 charge-transfer bands. For example, $Cs_2(TCNQ)_3$ has CT_1 at 11.1 kK and CT_2 at ca 5 kK (17,20).

Examination of the nujol mull spectrum of CuTCNQ salt (Fig. 1c) reveals bands centered at ca 430, 640 and 1100 nm. The 430-nm band has some vibronic structure and undoubtedly is the LE_2 band, which is of the same nature as the 415-nm band of the solution spectrum. Tanaka, et al (25) have estimated that a pure CT_1 band ($\sim$ 830 nm) occurs in the same region as a pure LE_1. Coupling between CT_1 and LE_1 causes splitting of the energy levels such that CT_1 moves to lower energy and LE_1 to higher energy. So, the 640-nm band of CuTCNQ salt is assigned to LE_1, which corresponds to the red band system of the solution spectrum, and the 1100-nm peak is attributed to the CT_1 charge transfer between two $TCNQ^-$ ions. This CT_1 assignment is in accord with the reported semiconductive properties of crystalline CuTCNQ, $\sigma = 1 \times 10^{-2} \Omega^{-1}$ cm^{-1} (26).

The spectrum of the CuTCNQ thin film, shown in Fig. 1b, represents a situation that is intermediate between that of the dilute solution (Fig. 1a), where the $TCNQ^-$ ions are well separated, and that of the crystalline CuTCNQ (Fig. 1c), where neighboring $TCNQ^-$ ions can interact significantly. To some extent the thin film spectrum resembles that of dimer-type $TCNQ^-$, reported by Boyd and Philips (18), and is consistent with dimer- or n-mer formation, effectively, in the thin films. The 390-nm band is clearly of LE_2 type, while the low energy region is dominated by a very broad absorption which can be

assigned to LE_1 and CT_1 bands in light of the preceding discussion. Although the latter bands are not completely separate, the LE_1 band is near 690 nm and the CT_1 is at ca 900 nm. Since there is no peak near 1100 nm, we assume that in thin films the coupling between CT_1 and LE_1 is not as strong as it is for the crystalline salt so CT_1 and LE_1 do not split as much as they do in the crystal.

The source wavelengths of the main Raman studies reported here are noted on Fig. 1. The 476.5-nm line corresponds to the minimum in absorption for the thin film, whose spectrum is shown in Fig. 1b.

For the purpose of comparisons, the Raman spectra of TCNQ° were measured at the various excitation wavelengths, so its absorption spectrum in solution and nujol mull were obtained and are given in Fig. 2. The solution exhibits the well known, strong peak at 393 nm (16,30), which is assigned to the $^1A_g \rightarrow {}^1B_{3u}$ (long-axis polarized) transition (5,30,31). In the solid state the band is broad and assymetric, with peaks at 450, 410 and 342 nm, which we associate with the polarized absorption bands of TCNQ crystals at 424, 402 and 340 nm (31). Hiroma, et al (31) attributed the structure from 370 to 435 nm to intermolecular charge transfer between two TCNQ° units, and the 340-nm band to an intramolecular transition.

Note that the excitation wavelengths fall essentially in the same electronic transition for TCNQ powder, but that in CuTCNQ powder they fall within two different absorption bands. Excitation also occurs at the absorption minimum in the case of the thin films.

Raman Spectra

The Raman spectra of CuTCNQ were measured on samples prepared by the three different methods described in the Experimental Section. The thick (ca 3-5 μm) polycrystalline films of CuTCNQ that were prepared by dipping Cu foils in TCNQ solution, and the KBr pellets of the CuTCNQ crystalline salt

powder that was prepared from CuI gave essentially the same spectra with all excitation wavelengths. For that reason, these forms of CuTCNQ will be referred to hereafter as the CuTCNQ salt, with electronic absorption spectrum given by Fig. 1c.

The Raman spectra of CuTCNQ salt measured with several exciting lines are presented in Fig. 3. It is clear that resonance Raman spectra excited by the 457.9-, 476.5-, and 514.5-nm lines are all similar, with minor differences in relative intensities, as may be expected from the fact that these three wavelengths fall in the same (blue band) electronic absorption region of the CuTCNQ salt. As the excitation changes from 457.9 to 514.5 nm, the 1203-, 980-, and 734-nm cm^{-1} bands decrease in relative intensity.

Excitation in the red band system, with the 632.8-nm line, gives quite a different spectrum in which the 980- and 734-cm^{-1} bands are very weak but the 1375-cm^{-1} band is the second strongest of the spectrum. Observing their dependences on excitation wavelength, it is clear that the relative intensity of the 1375-cm^{-1} band follows the red band absorption while that of the 734-cm^{-1} peak follows the blue band system. The observed enhancement selectivity is due to the fact that these modes are coupled differently to the two different electronic excitations. To illustrate this point we refer to the visible spectrum of solid TCNQ (Fig. 2b) and note that all of the excitation lines marked there fall in the same band system. These lines were used to measure the solid state (powder) Raman spectra of TCNQ presented in Fig. 4. These resonance Raman spectra are quite similar to each other and to reported solution Raman spectra of $TCNQ^{\circ}$ excited with the 488.0 (32) and 647.1 nm lines (21).

Based on the vibrational analysis of $TCNQ^{-}$ (10,11) and data on other TCNQ salts (11,21) we assign the bands of CuTCNQ at 2205, 1603, 1375, 1203, 980, 734, 616 and 341 cm^{-1} to toally symmetric modes (A_g), whose analogous bands in $TCNQ^{\circ}$ are at 2223, 1598, 1451, 1204, 948, 710, 600 and 333 cm^{-1}. Thus, the

resonance Raman spectra of CuTCNQ-powder are completely dominated by the A_g modes of $TCNQ^-$, and furthermore they show selectivity in resonance enhancement even among the totally symmetric modes, for example the ones at 1375 and 734 cm^{-1}.

The electronic absorption spectrum of thin CuTCNQ film (Fig. 1b) shows a displaced absorption minimum relative to that of the salt in Fig. 1c. As can be seen there, excitation of thin films with the 476.5- and 514.5-nm lines would permit measurement of the essentially non-resonance spectrum of CuTCNQ thin films. For this purpose thin CuTCNQ films (< 0.5 μm), prepared by the evaporation method on Al substrate, were used. The absorption characteristics of these films are similar to those of analogous thin films on fused silica shown in Fig. 1b, but films on Al were used for Raman measurements because the spectra obtained with thin films on fused silica (especially with the 514.5 line) are a superposition of the spectra of both CuTCNQ and fused silica. The CuTCNQ part of the Raman spectrum of the film on SiO_2 is the same as that of the CuTCNQ thin film on Al.

The Raman spectra of CuTCNQ thin films measured with four different excitation lines are shown in Fig. 5. Comparing these spectra with corresponding ones of CuTCNQ salt (Fig. 4) it is found, first that the 632.8-nm spectra are nearly the same because the 632.8-nm line falls in the red band system of both the film and salt. The spectra obtained with the 457.9-nm line also are similar, again because this excitation line is in the blue band of salt and the thin film. So, both 632.8 and 457.9 nm spectra of thin films can be regarded as resonance Raman spectra.

The spectra obtained with the 476.5- and 514.5-nm lines are remarkably different from the 632.8- or 457.9-nm line spectra, as far as the number of bands and their relative intensities are concerned. All the totally symmetric modes (A_g) present in the spectra of salt or thin films (excited with 632.8 and 457.9 nm lines) are still present, together with some other bands, which

are either absent or very weak in the resonance Raman spectra of the salt or the thin film. For example the bands at 958, 1180, 1268 and 1632 cm^{-1} are weak in the 457.9 nm spectrum of the thin film or the corresponding spectrum of the salt. The above mentioned peaks and those at 2221, 1327, 1012, and 365 cm^{-1} are of similar or higher intensity than the A_g mode peaks in the 514.5-nm line spectrum. It is very characteristic that in the 476.5-nm line spectrum of the thin film, the totally symmetric modes gain intensity against the rest of the bands of the spectrum. We believe that all the above facts help to draw the conclusion that excitation of thin films with the 514.5 nm line gives the non-resonance spectrum of CuTCNQ, while excitation with the 476.5 nm line meets preresonance conditions, so that the totally symmetric modes are the most intense ones. Excitation with 632.8 and 457.9 nm lines gives the resonance Raman spectra which are completely dominated by totally symmetric modes.

Jeanmaire and Van Duyne (21) initially and Khatkale and Devlin (11) more recently indicated doubts about the origin of some of the bands that Chi and Nixon (33) reported in their Raman spectra of RbTCNQ and KTCNQ prepared by the metal iodide reaction. Specifically the bands reported (33) at 2214, 1622, 1330, 1280, 1181, 1005, 962, 725 and 356 cm^{-1} were taken to be similar to the Raman bands at 2214, 1638, 1327, 1281, 1174, 1000, 963, 735 and 349 cm^{-1} that have been reported to be characteristic bands of α,α-dicyano-p-toluoyl cyanide ($DCTC^-$) in CH_3CN solution (34). It was concluded (11,21) that the above bands assigned by Chi and Nixon to non-totally symmetric modes were really due to the presence of $DCTC^-$, an oxidation product of $TCNQ^{-2}$. On the basis of this argument one also might conclude that the bands of CuTCNQ film at 2221, 1632, 1327, 1268, 1180, 1012, 958 and 365 cm^{-1} are due to $DCTC^-$.

Thus, we must examine the support for our assignment. First, the thin CuTCNQ films were prepared by heating Cu° and TCNQ° in vacuum or in a dry box filled with Ar gas. Production of oxidation products is unlikely under these conditions, and the visible spectra of the blue-green films prepared by the above method do not show a peak at 480 nm (Fig. 1b), where $DCTC^-$ has its strong absorption maximum in solution (34). In fact, the thin film spectrum shows an absorbance minimum at about 480 nm. While this result is consistent with the absence of $DCTC^-$, it is possible that it is present but that its absorbance maximum in the solid state is shifted from its value in solution. Alternatively, it is possible that the $DCTC^-$ absorbance band is present at 480 nm but that its absorbance is not as high in thin films as would be expected. In addition, it is possible that $DCTC^-$ is not present as a result of the preparation, but that it is produced locally under laser irradiation in air.

Let us then suppose that the Raman bands in question are due to $DCTC^-$ and that it has an absorbance maximum at ca 480 nm. Then the 476.5-nm laser line source would be closest to the maximum absorbance of $DCTC^-$, while the laser lines at 514.5 and 457.9 nm would come at frequencies at which the $DCTC^-$ absorbance is approximately the same, as judged from the solution spectrum (34). If this were the case we might expect that these Raman modes would have their maximum relative intensities with the 476.5-nm line and similar but lower intensities with the other two lines (514.5 and 457.9 nm). However, their relative intensities actually decrease systematically as the source wavelength decreases from 514.5- to 457.9-nm. At this point one could suggest that the absorption maximum of $DCTC^-$ in the solid state is actually at longer wavelength than 480 nm, in fact closer to the 514.5-nm line, and that the observed trend in relative Raman intensities is the one expected on the basis of resonance enhancement within an

electronic transition in the ca 510-600 nm region. If this were true, though, we would expect at least that these Raman bands would appear in the spectrum excited by the 632.8-nm line. However, they do not appear at all in that spectrum. If the absorption maximum of $DCTC^-$ in the solid state were shifted to shorter wavelength than 480 nm (that is closer to 457.9 nm) then the expected relative intensity trend would be the opposite to what is observed.

Of course all of the above arguments are based on the assumption that the Raman spectrum of $TCNQ^-$ itself does not change significantly with excitation by the 514.5 to 457.9 nm lines, as is the case with CuTCNQ power (Fig. 3). In that way the A_g modes of $TCNQ^-$ are used as an internal standard in comparing the changes upon excitation on the intensities of the bands in question. However, if the spectrum of $TCNQ^-$ changes significantly upon excitation in this region then the exclusion of the presence of $DCTC^-$ becomes more difficult. But even that case proves the point that the 514.5 nm line excites the non-resonance Raman spectrum of $TCNQ^-$ (in thin films), while the 476.5-nm line excites the pre-resonance and the 457.9 and 632.8 nm lines excite resonance Raman spectra of $TCNQ^-$.

Photoinduced transition $TCNQ^- \rightarrow TCNQ^\circ$

It was reported recently (4) that reversible and rapid bistable electrical switching was achieved in chemically prepared films of CuTCNQ on Cu substrates. A threshold field strength of about 1×10^4 V cm^{-1} was required for electrical switching from a high to a low impedance state. We have studied the mechanism of this electrical switching in situ by Raman spectroscopy and found that while the high impedance state is Cu^+TCNQ^- the low impedance state is characterized by the presence of both $TCNQ^\circ$ and Cu^+TCNQ^- (1). This is consistent with the notion that the presence of $TCNQ^\circ$ among the $TCNQ^-$ ions along the 1-D stacks is what makes the impedance very low immediately after electrical switching.

In the process of measuring the Raman spectra of various forms of CuTCNQ

(as well as AgTCNQ) we observed that for laser powers higher than some average levels the characteristic Raman peaks of TCNQ° were obtained together with that of $Cu^{+}TCNQ^{\tau}$ (2,3). The degree to which the phototransformation of $TCNQ^{-}$ to TCNQ° proceed depends on the power of the light, the duration of exposure and the specific form of the sample. Thus, both partial and complete transformations were effected. Partial transformations of CuTCNQ and AgTCNQ were shown to yield materials which are spectroscopically identical to the low impedance form of each. The partially transformed materials return to the metal-TCNQ form spontaneously but, at 25°C, slowly. This constitutes a memory effect which also is exhibited in the case of electric-field-induced transformation. The complete transformation leads to formation of metallic regions in the exposed areas, when conditions permit the TCNQ° to be removed (sublimed) and the metal to remain. Photoinduced transformations were effected with laser light at frequencies within both electronic systems of $TCNQ^{\tau}$ (3). Similar phototransformation phenomena were also reported in CuTCNQ and AgTCNQ (35).

The light-induced transformation phenomena described above are very similar to phenomena observed under the action of an electric field (1,4) in that in both cases mixed valence species are formed, and thus the following equation may be used to describe the process:

$$(M^{+}TCNQ^{\tau})_{x} \xrightleftharpoons{h\nu} M^{\circ}_{y} + TCNQ^{\circ}_{y} + (M^{+}TCNQ^{\tau})_{x-y} \qquad (1)$$

The threshold for electrical switching in chemically prepared CuTCNQ films has a typical value of $E = 1 \times 10^{4}$ V cm^{-1}. If we take the static dielectric constant of CuTCNQ to be ε, then the effective electric field becomes $E_{eff} = (1/\varepsilon)E$. The static dielectric constant, ε, can be approximated by the microwave dielectric constant of KTCNQ, measured by Heeger and coworkers to be $\varepsilon = 6$ (36). Thus the effective electric field for electrical switching is $E_{eff} = 1.7 \times 10^{5}$ V m^{-1}. On the other hand the electric field E, of an electromagnetic wave is related

to the power P, transmitted through a unit area by (37):

$$E = (2P)^{1/2}(\mu_o/\epsilon_o)^{1/4} \qquad (2)$$

where ϵ_o is the permittivity of free space (8.855×10^{-12} Farad/m) and μ_o is the permeability of free space (1.257×10^{-6} Henry/m). For phototransformation of CuTCNQ chemically prepared films the power threshold has a typical value $P \approx 5 \times 10^4$ W m^{-2} (3). Thus the electromagnetic field for optical transformation is $E \approx 6 \times 10^3$ V m^{-1}, that is about 25 times weaker than the electric field threshold for electrical switching.

Both thermal and electronic effects could be responsible for causing the phototransformation. To explore the possibility of thermal effects being responsible for the transformation, several experiments were performed. First, we estimated the temperature rise due to local heating by the laser beam. By using the 476.5 nm line at 8 mW/mm^2 (just below the threshold for phototransformation) and CuTCNQ powder, the local temperature, estimated from the anti-Stokes to Stokes intensity ratio of the 734- and 1603-cm^{-1} bands, was found to be about 160°C. This is below the decomposition temperature for CuTCNQ ($\sim$ 300°C), but much higher than room temperature. Second, exposures of the materials to the laser beam for extended periods of time, but at powers less than the threshold values, did not cause the transformation. However, increase of the power to the threshold value causes the phototransformation to occur immediately. That indicates the threshold nature of these metal-TCNQ materials. Linear materials would exhibit transformation phenomena for lower power levels but longer exposures. Third, Raman spectra of CuTCNQ powder taken as a function of temperature, at low power, gave no evidence of TCNQ° production as a result of heating at temperatures as high as 290°C. Finally, the observation that metal (Cu,Ag) and TCNQ° react upon heating ($\sim$100°C) to form M^+TCNQ^- (1,3) shows that the latter is the thermally stable form, and, furthermore, that the reverse reaction Eq. (1) can be speeded up (shorter memory) upon heating.

All the evidence presented above exclude the thermal effects as the sole cause of the transformation. On the other hand, illumination of the metal-TCNQ materials with the laser light causes electronic transitions of $TCNQ^{\pi}$ to higher electronic states and this makes it easier for one electron to leave the anion radical and be captured by the metal cation. Thus, the phototransformations studied seem to be due to photoinduced electronic transitions, rather than thermal effects.

Frequency Calculations of the A_g Modes of TCNQ Ion-Radicals

It is well known that reduction of $TCNQ^{\circ}$ to $TCNQ^{-}$ or $TCNQ^{=}$ produces substantial vibrational frequency shifts due to electronic structural changes. These shifts are most pronounced for totally symmetric modes of the charged species. Since the electronic structures of $TCNQ^{\circ}$, $TCNQ^{-}$ and, to a lesser extent, of $TCNQ^{=}$ are known, it should be possible, in principle, to relate them to force constants and calculate the frequencies of vibration of the anion-molecules. In normal coordinate analyses of such similar species it is always possible to reproduce the spectral shifts by changing the force constants. This was shown in the case of $TCNQ^{-}$, for example, whose frequencies were calculated by changing some of the diagonal elements of $TCNQ^{\circ}$ (10,14). In later work by Van Duyne and coworkers (21,38) and Krogh-Jepsersen and Ratner (7) an attempt was made to draw a correlation between bond order changes and the vibrational frequency shifts, but only qualitative conclusions were drawn. In this section we actually calculate the vibrational frequencies of the anion radicals to the extent possible using results of reported molecular orbital calculations.

The method we used is similar to that employed initially by Yamaguchi et al (39) to calculate the vibrational frequencies of biphenyl negative ion (BP^{-}) and later by Tzinis (40) to calculate some frequencies of dopped polyparaphenylene ($PPP^{-\delta}$ or $PPP^{+\delta}$). In this approach the bond strengths (force constants) of various CC bonds have been expressed by Coulson and

Longuet-Higgins (41,42) as follows:

$$K_r = \sigma(1-P_r) + kP_r + \frac{1}{2}\left[\frac{k\sigma(s-d)}{\sigma(1-P_r)+kP_r}\right]^2 \pi_{r,r} \qquad (3)$$

where the symbols used are: K_r the force constant of bond r, P_r the π-bond order of bond r, s and d the standard lengths of pure single (C-C) and pure double (C=C) bonds respectively, σ and k the force constants of single (C-C) and double (C=C) bonds respectively and $\pi_{r,r}$ the self polarizability of bond r. Equation (3) has been derived mainly for CC bonds but it can be used to account for CN bonds as well. In this case the pure C=N bond corresponds to the C-C bond and pure C≡N to C=C bond.

The π-bond order P_r is given by the familiar expression:

$$P_r = P_{\mu\nu} = \sum_{k=1} b_k C_{k\mu} C_{k\nu} \qquad (4)$$

where atoms μ and ν define bond r, b_k is the number of electrons in the ψ_k molecular orbital and $C_{k\mu}$, $C_{k\nu}$ are the Hückel coefficients giving the contribution of the ϕ_μ and ϕ_ν atomic orbitals to the ψ_k molecular orbital.

The self polarizability $\pi_{r,r}$ of bond r is a special case of the mutual polarizability between two bonds given in ref. (42) and can be written as:

$$\pi_{r,r} = \pi_{\mu\nu,\mu\nu} \sum_{j=1} \sum_{k\neq j} b_j \frac{(C_{\mu j}C_{\nu k}+C_{\mu k}C_{\nu j})^2}{\varepsilon_j - \varepsilon_k} \qquad (5)$$

where ε_j is the energy of the j^{th} molecular orbital. This equation is written as follows for TCNQ°, $TCNQ^-$ and $TCNQ^=$:

$$TCNQ^\circ: \quad \pi_{r,r} = \sum_{j=1}^{8} \sum_{k=9}^{16} b_j \frac{(C_{\mu j}C_{\nu k}+C_{\mu k}C_{\nu j})^2}{\varepsilon_j - \varepsilon_k} \qquad (6)$$

$$TCNQ^-: \quad \pi_{r,r} = \sum_{j=1}^{8} \sum_{k=9}^{16} b_j \frac{(C_{\mu j}C_{\nu k}+C_{\mu k}C_{\nu j})^2}{\varepsilon_j - \varepsilon_k} + \sum_{k\neq 9}^{16} \frac{(C_{\mu 9}C_{\nu k}+C_{\mu k}C_{\nu 9})^2}{\varepsilon_9 - \varepsilon_k} \qquad (7)$$

$$TCNQ^=: \quad \pi_{r,r} = \sum_{j=1}^{9} \sum_{k=10}^{16} b_j \frac{(C_{\mu j}C_{\nu k}+C_{\mu k}C_{\nu j})^2}{\varepsilon_j - \varepsilon_k} \qquad (8)$$

Using eqs. (3), (4), and (5) we can calculate the force constants K_r of the different kinds of bonds. Calculation of the frequencies of different normal modes would require the knowledge of an effective force constant K_i for the i^{th} normal mode. The contributions of the various K_r's to a particular K_i is taken as being equal to the potential energy distribution $(PED)_{r,i}$ of bond r to the i^{th} normal mode, so we write:

$$K_i = \sum_r (PED)_{r,i} K_r \qquad (9)$$

where the summation is over the kind of bonds.

Reduction of TCNQ° makes K_i (neutral) change to K_i (ion) and ν_i (neutral) to ν_i (ion) where ν_i is the frequency of the i^{th} normal mode. In the simple harmonic oscillator case it is easy to show that the frequency of the charged species ν_i (ion) will be:

$$\nu_i(\text{ion}) = \nu_i \text{ (neutral)} \left[1 + \frac{\Delta K_i}{[2\pi C \nu_i(\text{neutral})]^2 \mu} \right]^{1/2} \qquad (10)$$

where $\Delta K_i = K_i$ (ion) $- K_i$ (neutral), C is the speed of light and μ the reduced mass.

Bond lengths and force constants of the various bonds are taken from ref. (43) and are included in Table 1. Hückel coefficients and MO energies are obtained from the molecular orbital calculation on TCNQ° and $TCNQ^-$ performed by Lowitz (5). Results designated in (5) as set 1 (TCNQ°) and as set 3 ($TCNQ^-$) are employed. For $TCNQ^=$ we used the results of $TCNQ^-$ by simply fitting an extra electron to the ψ_9 molecular orbital. Bond orders calculated by eq. (4) and bonds self polarizabilities calculated by eqs. (6), (7) and (8) are given in Table 2. The numbering scheme used is shown in Fig. 6, where also the various symbols used for PED are included. The force constants of various bonds K_r are also tabulated. The contribution of the bond self polarizability $\pi_{r,r}$ to K_r is always negative and combined with that of the bond order produce

a very interesting trend in K_r. Namely the strengths of bonds 1-2, 5-7, and 9-13 are reduced upon ionization while the strengths of the single bonds 1-5 and 7-9 are increased by increasing the charge on TCNQ°.

The potential energy distribution (PED) required to calculate the effective force constants K_i is given in Table 3. Since the results of various normal mode analyses for TCNQ° and $TCNQ^-$ have indicated that the vibrational scheme for the monoion is very similar to that of the neutral molecule, we assumed for all species (TCNQ°, $TCNQ^-$, and $TCNQ^=$) the PED of TCNQ° obtained from ref. (8). From the last two columns of Table 3 it is clear that for pure or nearly pure bending modes the observed frequency changes upon ionization are small. For that reason we set PED weighing factor equal to zero for the bending coordinates. The calculated force constant changes, K_i are given in Table 3 and have been used to calculate the frequencies of totally symmetric modes of $TCNQ^-$ and $TCNQ^=$. The calculated frequencies are given in Tables 4 and 5, where they are also compared with experimental results. With the exception of mode ν_3 the rest of the calculated frequencies satisfactorily compare with the experimental ones. This is particularly true for $TCNQ^-$ where the direction and the magnitude of the frequency shifts is successfully predicted. Some of the modes, i.e. ν_2, ν_4, ν_5, and ν_8 have calculated frequencies exactly the same as the experimental ones. Overall, the average absolute error for $TCNQ^-$ is estimated to be 0.7% which is very satisfactory. For $TCNQ^=$ the calculated frequencies are less accurate, but nevertheless the estimated average error is about 2%, which can be regarded as acceptable if we recall that the molecular orbital parameters and PED used for $TCNQ^=$ were extrapolations or the same used for TCNQ° and $TCNQ^-$.

We already have mentioned that the degree of charge-transfer from donor to TCNQ molecule is directly related to the conductivity of the ion-radical salts.

This is so because ρ determines the band filling, and thus it allows the study of the relation between band filling and physical properties. Matsuzaki et al (15) have observed a linear dependence of the ν_4 frequency on the formal charge on the TCNQ moiety (ρ) for a number of TCNQ salts. Here we test our model to see if it predicts this experimentally established linear relationship between ρ and the ν_4 frequency. Since we have calculated ν_4 for $\rho = 1$ and $\rho = 2$ we extend the calculation to that for $\rho = 0.59$, the established degree of charge transfer for TTF-TCNQ (28). For the calculation the molecular orbital parameters of $TCNQ^-$ (Lowitz, set 3) have been utilized by simply replacing the 17^{th} electron of $TCNQ^-$ in the ψ_9 molecular orbital by 0.59 electrons. Bond orders, bond self polarizabilities and force constants for $TCNQ^{-0.59}$ are shown in Table 6.

The results for the force constants K_r are very nicely in between those of $TCNQ^\circ$ and $TCNQ^-$ as expected. The calculated frequency for the ν_4 mode is 1398 cm^{-1}, which compares reasonably well with the experimental one for TTF-TCNQ of 1420 cm^{-1} (15). To find whether or not our model predicts the linear dependency of ν_4 on ρ we have plotted in Fig. 7 the calculated ν_4 frequencies for $TCNQ^{-0.59}$, $TCNQ^{-1}$, and $TCNQ^=$, as a function of the degree of charge transfer. Indeed, a linear dependence of ν_4 on ρ is shown.

Resonance Raman Intensity Calculations for $TCNQ^-$

The resonance Raman phenomena shown to be exhibited by CuTCNQ, especially the selectivity in resonance enhancement among A_g modes, are also observed with other TCNQ salts as well. This is characteristically shown in Fig. 8 for AgTCNQ and LiTCNQ. The Raman spectra obtained by excitation in the two electronic bands of $TCNQ^-$ are very similar to the corresponding ones of CuTCNQ salt. Thus, the calculations and discussion presented in this part refer to $TCNQ^-$ in general and are not limited to CuTCNQ.

The resonance Raman effect has been treated theoretically by a number of investigators (44-47) and general expressions have been derived for the frequency dependence of the Raman intensity. In the simple case in which only one or two excited electronic states are involved, Albrecht and Hutley (45) have shown that the resonance Raman intensity is proportional to the square of the weighted sum of the factors F_A and F_B given by:

$$F_A = \nu^2(\nu_e^2 + \nu_o^2)/(\nu_e^2 - \nu_o^2)^2 \qquad (11)$$

and

$$F_B = 2\,\nu^2(\nu_e\nu_s + \nu_o^2)/(\nu_e^2 - \nu_o^2)(\nu_s^2 - \nu_o^2) \qquad (12)$$

where $\nu = \nu_o - \nu_k$, ν_k is the frequency of the k-th mode, ν_o is the excitation frequency, and ν_e and ν_s are the frequencies associated with the transition from the ground to the excited electronic state in question. The A term describes the frequency dependence of the intensity, if the k-th vibrational mode is coupled to a single electronic transition, (Franck-Condon coupling) and the B term applies if the mode is enhanced through a mixing of two electronic transitions, (Herzberg-Teller coupling).

This approach was used by Klein and coworkers (48) in their study of the resonance Raman spectra of LiTCNQ solutions. They observed that excitation in the blue-band results in B-type enhancement due to vibronic mixing of at least two electronic transitions, but excitation in the red-band shows A-type enhancement, due to single electronic excitation in this region. This is in agreement with the results of the molecular orbital studies discussed earlier. If we use the factor F_A^2 to predict the intensities of the various modes, for excitation with the 632.8-nm line, the relative intensities obtained are not in agreement with the experimental ones. Thus expression (11) and (12) are useful for distinguishing between different types of resonance enhancement but are not adequate to predict relative intensity enhancement. In this part we

calculate the resonance enhancement of $TCNQ^-$, excited in the red-band system, by calculating the coupling of different A_g modes with the electronic excitation. Similar calculations for excitation in the blue-band system are more difficult, because they require more knowledge of the excited electronic states than is available from the spectrum which rises from the overlap of the different electronic excitations.

For Franck-Condon type resonance enhancement the scattered intensity depends on the overlap <gj/ev><ev/gi>, where gj and gi are the ground vibronic states and ev is the excited vibronic state, with g and e being the ground and excited electronic states respectively. If the internuclear distances in the two vibronic states gj and ev are very similar then the vibronic wave functions are nearly orthogonal and the integral <gj/ev> is small. If the molecular configuration in the excited electronic state is much different than that of the ground state then the overlap is exceptionally high and resonance Raman scattering occurs. However, only those normal modes which couple with the electronic excitation are resonantly enhanced. For CuTCNQ this is clearly demonstrated by the 980 and 734 cm^{-1} bands, which are resonantly enhanced in the blue-band system, but not in the red-band system.

The Franck-Condon term of the scattering tensor for a diatomic molecule, of fundamental frequency ν_j, is given by (4):

$$\alpha_{\rho\sigma} = \frac{(\sqrt{2}\pi/h)(M_\rho)^o_{ge}(M_\sigma)^o_{ge}\nu_j(\nu_j/h)^{1/2}\cdot\Delta Q}{(\nu_e - \nu_o + i\gamma_e)(\nu_e + \nu_j - \nu_o + i\gamma_e)} \qquad (13)$$

where $\alpha_{\rho\sigma}$ is the $\rho\sigma$-th element of the polarizability tensor, $(M)_{ge}$ is the moment of transition, γ_e is the damping constant for the electronic state e and ΔQ is the normal coordinate change during the electronic excitation. It has been shown (39) that equation (13) can be used for polyatomic molecules as well, under the assumption of large damping constant and near-resonance conditions.

Depolarization ratio measurements of A_g modes of $TCNQ^-$ in the red-band system (21,50) have shown that it is equal to ca 0.33 for each. This value indicates that only one diagonal element of the scattering tensor contributes significantly to the intensity, and that this is the α_{xx} component (50). By simplifying equation (13), for large damping constant and near-resonance conditions, the Raman intensity of the N-th normal mode of $TCNQ^-$ can be written as:

$$I_N = \text{constant } \alpha_{xx}^2 = \text{constant } \nu_N^3 \Delta Q_N^2 \qquad (14)$$

Here ν_N is the frequency of the N-th normal mode and ΔQ_N represents the change of this normal mode caused by the electronic transition, through the distortion of the molecular geometry. Thus calculation of I_N requires the knowledge of ΔQ_N.

The Cartesian coordinate displacements of the atoms caused by a normal mode of vibration can be written in a matrix form as (51):

$$X = TQ \qquad (15)$$

where the Cartesian, X and normal coordinate matrix, Q are column matrices and T describes their transformation. The physical meaning of this expression is that for unit normal coordinate displacements the atomic Cartesian displaceemnts are simply given by the elements of matrix T. If we now assume that the vibrational scheme of $TCNQ^-$ is similar to that of TCNQ°, given in ref. 52, then this normal mode scheme can be directly used to find the elements of the T matrix. Now let ΔX be the matrix of the atomic Cartesian displacements caused by the electronic transition. Then the resulting ΔQ will be:

$$\Delta Q = T^{-1} \Delta X, \qquad (16)$$

and for the N-th normal mode:

$$\Delta Q_N = \sum_{i=1}^{2n} T_{iN}^{-1} \quad X_i \qquad (17)$$

The summation is only over the x and y Cartesian displacements since we are deal-

ing with in plane A_g modes. The quantities required to calculate ΔQ_N are the Cartesian displacements, ΔX_i, due to the electronic transition.

As discussed earlier the red-band system is attributed to the $^2B_{2g} \rightarrow {}^2B_{1u}{}^{(1)}$ electronic transition which is achieved by the $\psi_8 \rightarrow \psi_9$ electronic excitation. Using the molecular orbital results for $TCNQ^-$, with two electrons in ψ_9 MO and one electron in ψ_8 the various bond orders in $^2B_{1u}{}^{(1)}$ excited electronic state can be calculated. Then the electronic population changes due to the electronic excitation are represented by the bond order difference, ΔP_r, between excited and ground electronic state. The corresponding changes of the equilibrium bond lengths can be estimated by the empirical formula (43).

$$\Delta r = -B\Delta P_r (A^\circ) \qquad (18)$$

where the parameter B is equal to 0.176 for CC and 0.175 for CN bond. The results of the calculation are given in Table 7 and are used to estimate the molecular geometry in the $^2B_{1u}{}^{(1)}$ electronic state. Equilibrium bond lengths and angles of the ground electronic state for $TCNQ^-$ are obtained from ref. 53. The molecular geometries in $^2B_{2g}$ and $^2B_{1u}{}^{(1)}$ electronic states are shown in Figure 9. The geometry of the ground state is drawn in scale, but that of the excited state is exaggerated to show the direction of the atomic displacements involved during the electronic excitation. Thus the Cartesian displacements, ΔX_i, can be calculated now from that geometrical data, and thus ΔQ_N can be calculated by means of equation (17).

At this point we note that the intensity I_N, calculated as described above must be temperature- and frequency-corrected so that it can be compared with the experimental one (54):

$$I_N = \text{constant} \; \frac{(\nu_o - \nu_N)^4}{\nu_N [1-\exp(-hC\nu_k/T)]} \; \alpha_{xx}^2 =$$

$$= \text{constant} \; \frac{(\nu_o - \nu_N)^4}{[1-\exp(-hC\nu_k/T)]} \; \nu_N^2 \, \Delta Q_N^2 \qquad (19)$$

where ν_o = 632.8 nm = 15803 cm^{-1}, T = 298°K, and C is the speed of light. The intensities calculated by using equation (19) are normalized relative to that of the ν_3 mode. The calculated resonance Raman spectrum is shown in Figure 10, where the experimental one (for CuTCNQ) is also given. The 1603 cm^{-1} band is successfully predicted as the most intense band of the spectrum, while the ones at 980 and 734 cm^{-1} are correctly predicted as not enhanced, for this excitation. The relative intensities of the 2205- and 616-cm^{-1} bands are almost the same as that of the observed spectrum. The 1375 cm^{-1} band is not predicted to be as much enhanced as it really is, while the 1203 cm^{-1} band is stronger than the observed one. Overall, the agreement between the calculated and experimental spectrum is good and it confirms that the enhancement in the red-band is of Franck-Condon type.

Acknowledgments

This work was supported by the Office of Naval Research and the Materials Research Laboratory of Brown University through the National Science Foundation. We gratefully acknowledge discussions with Vincent Mattera of Brown University and Dr. Costas Tzinis of Bell Laboratories.

References

1. E.I. Kamitsos, C.H. Tzinis and W.M. Risen, Jr., Solid State Commun., 42, 561 (1982).

2. W.M. Risen, Jr., and E.I. Kamitsos, Patent submission, Brown University, March 10, 1982.

3. E.I. Kamitsos and W.M. Risen, Jr., Solid State Commun., 45, 165 (1983).

4. R.S. Potember, T.O. Poehler and D.O. Cowan, Appl. Phys. Lett., 34, 405 (1979).

5. D.A. Lowitz, J. Chem. Phys., 46, 4698 (1967).

6. A. Bieber and J.J. Andre, Chem. Phys., 5, 166 (1974); 7, 137 (1975).

7. K. Korgh-Jespersen, M.A. Ratner, Theoret. Chim. Acta. 47, 283 (1978).

8. A. Girlando and C. Pecile, Spectrochim. Acta, 29A, 1859 (1973).

9. T. Tekenaka, Spectrochim. Acta, 27A, 1735 (1971).

10. R. Bozio, A. Girlando and C. Pecile, J. Chem. Soc. Farad. Trans. II, 71, 1237 (1975); R. Bozio, I. Zanon, A. Girlando and C. Pecile, J. Chem. Soc. Farad. Trans. II, 74, 235 (1978).

11. M.S. Khatkale and J.P. Devlin, J. Chem. Phys., 70, 1851 (1979).

12. A. Girlando, R. Bozio and C. Pecile, Chem. Phys. Lett., 25, 409 (1974).

13. J.B. Torrance, Acc. Chem. Res. 12, 79 (1979).

14. R. Bozio and C. Pecile in "The Physics and Chemistry of Low-Dimensional Solids," ed. by L. Alcacer, D. Reidel Publishing Co., Dordrecht, Boston, and London, 1980.

15. S. Matsuzaki, R. Kuwata and K. Toyoda, Solid State Commun., 33, 403 (1980).

16. L.R. Melby et al., J. Am. Chem. Soc., 84, 3374 (1962).

17. J. Tanaka et al., Bull. Chem. Soc. Japan, 49, 2358 (1976).

18. R.H. Boyd and W.D. Phillips, J. Chem. Phys., 43, 2927 (1965).

19. Y. Iida, Bull. Chem. Soc. Japan, 42, 71 (1969).

20. S. Hiroma et al., Bull. Chem. Soc. Japan, 44, 9 (1971).

21. D.L. Jeanmaire and R.P. Van Duyne, J. Am. Chem. Soc., 98, 4029 (1976).

22. Y. Oahashi and T. Sakata, Bull. Chem. Soc. Japan, 46, 3330 (1973).

23. H. Kuroda, S. Hiroma, H. Akamatu, Bull. Chem. Soc., Japan, 41, 2855 (1968).

24. M. Morinaga et al., Bull. Chem. Soc. Japan, 53, 1221 (1980).

25. J. Tanaka et al., in "Synthesis and Properties of Low-Dimensional Materials", ed. by J.S. Miller and A.J. Epstein, Annals. of the New York Academy of Science, NY (1978).

26. W.J. Siemons, P.E. Bierstedt and R.G. Kepler, J. Chem. Phys., 39, 3523 (1963).

27. J. Ferraris, D.O. Cowan, V. Walatka and J.H. Perlstein, J. Am. Chem. Soc., 95, 948 (1973).

28. R. Comes, in "Chemistry and Physics of One-Dimensional Metals", NATO ASI. Series B25, p 315, Plenum Press, NY (1977).

29. J.B. Torrance, B.A. Scott and F.B. Kaufmann, Solid State Commun., 17, 1363 (1975).

30. C.J. Eckhardt and R.R. Pennelly, Chem. Phys. Lett., 9, 572 (1971).

31. S. Hiroma, H. Kuroda and H. Akamatu, Bull. Chem. Soc. Japan, 43, 3626 (1970).

32. W.L. Wallance et al., J. Am. Chem. Soc., 101, 4870 (1979).

33. C. Chi and E.R. Nixon, Spectrochim. Acta, 31A, 1739 (1975).

34. M.R. Suchanski and R.P. Van Duyne, J. Am. Chem. Soc., 98, 250 (1976).

35. R.S. Potember, T.O. Poehler and R.C. Benson, Appl. Phys. Lett. 41, 548 (1982).

36. S.K. Khanna, A.A. Bright, A.F. Garito and A.J. Heeger, Phys. Rev. B10, 2139 (1974).

37. O.D. Jefimenko, "Electricity and Magnetism', Appleton-Century-Crofts, New York, 1966.

38. R.P. Van Duyne, et al., J. Am. Chem. Soc., 101, 2832 (1979).

39. S. Yamaguchi et al., J. Phys. Chem., 82, 1078 (1978).

40. C. Tzinis, Ph.D. Thesis, Brown University, 1981.

41. C.A. Coulson and H.C. Longuet-Higgins, Proc. Roy. Soc., 193A, 456 (1948).

42. C.A. Coulson and H.C. Longuet-Higgins Proc. Roy. Soc., 191A, 39 (1947).

43. M.J.S. Dewar and G.J. Gleicher, J. Chem. Phys., 44, 759 (1966).

44. A.C. Albrecht, J. Chem. Phys., 34, 1476 (1961); J. Tang and A.C. Albrecht, in "Raman Spectroscopy", ed. by H.A. Szymanski, Vol. 2, Plenum Press, NY (1970).

45. A.C. Albrecht and M.C. Hutley, J. Chem. Phys. 55, 4438 (1971).

46. W.L. Peticolas, L. Nafie, P. Stein and B. Faneoni, J. Chem. Phys., 52, 1576 (1970).

47. R.J.H. Clark and B. Stewart, Structure and Bonding, Vol. 36, Springer-Verlag, NY (1979).

48. W.T. Wozniak, G. Depasquali and M.V. Klein, Chem. Phys. Lett. 40, 93 (1976).

49. S. Kobinata, Bull. Chem. Soc. Japan, 46, 3636 (1973).

50. E.I. Kamitsos and W.M. Risen, J. Chem. Phys, 79, 477 (1983).

51. E.B. Wilson, J.C. Decius and P.C. Cross, "Molecular Vibrations", McGraw-Hill, NY (1955).

52. N.O. Lippari, et al., Int. J. Quantum Chem. Symposium, 11, 583 (1978).

53. C.J. Fritchie, Jr., and P. Arthur, Jr., Acta Cryst., 21, 139 (1966).

54. D.A. Long,"Raman Spectroscopy, McGraw-Hill, New York (1977).

Table 1. Bond lengths and force constants for CC and CN bonds.[a]

Bond	$s(10^{-8}cm)$	$d(10^{-8}cm)$	$\sigma(10^{5}dyn/cm)$	$k(10^{5}dyn/cm)$
CC	1.485	1.334	6.030	10.896
CN[b]	1.270	1.153	10.500	18.583

(a) Data is taken from ref.(43).

(b) s and σ refer to C=N, while d and k refer to C $\equiv$ N.

Table 2. Bond orders, P_r, bond self polarizabilities $\pi_{r,r}$, and force constants, K_r, for the various bonds of TCNQ°, $TCNQ^-$ and $TCNQ^=$.

Bond	P_r			$\pi_{r,r}(10^{10}\ erg^{-1})$		
	TCNQ°	$TCNQ^-$	$TCNQ^=$	TCNQ°	$TCNQ^-$	$TCNQ^=$
1-2	0.88874	0.79438	0.72711	-1.0462	-2.6066	-3.7279
1-5	0.34658	0.46100	0.53077	-4.5072	-4.7681	-4.3179
5-7	0.81176	0.63632	0.51421	-1.6755	-4.3077	-5.8706
7-9	0.26854	0.33118	0.36892	-4.2540	-5.3386	-5.6225
9-13	0.95824	0.92478	0.90891	-0.4246	-1.0692	-1.3839

	$K_r(10^5 dyn/cm)$		
Bond	TCNQ°	$TCNQ^-$	$TCNQ^=$
1-2	10.307	9.764	9.368
1-5	7.344	7.930	8.326
5-7	9.897	8.872	8.135
7-9	6.948	7.192	7.373
9-13	18.212	17.889	17.773

Table 3. Potential energy distribution (PED) and calculated effective force constant shifts.

Mode	[a]PED(%)	ΔK_i ($TCNQ^-$-TCNQ°) (10^5dyn/cm)	ΔK_i ($TCNQ^=$-TCNQ°) (10^5dyn/cm)	TCNQ° (cm^{-1})	CuTCNQ (cm^{-1})
ν_2	K_5(87)	-0.281	-0.420	2223	2205
ν_3	[b]K_1(56), K_2(21), H_3(17)	-0.181	-0.319	1598	1603
ν_4	K_1(30), K_3(59)	-0.767	-1.321	1451	1375
ν_5	H_3(81)	0	0	1204	1203
ν_6	K_2(45), K_4(21)	+0.315	+0.531	948	980
ν_7	K_2(32), K_4(17)	+0.229	+0.387	710	734
ν_8	K_4(23), H_6(43), H_7(18)	+0.056	+0.098	600	616
ν_9	H_4(18), H_6(18)	0	0	333	341

(a) PED obtained from (8).

(b) PED for ν_3 obtained from (11).

(c) K_i: stretch, H_i: bend

Table 4. Calculated and experimental frequencies (cm^{-1}) of A_g modes of $TCNQ^-$.

Mode	$TCNQ^-$ calc.	CuTCNQ	NaTCNQ[(a)]	RbTCNQ[(b)]	$TCNQ^-$(soln)[(c)]
ν_2	2206	2205	2193	2206	2192
ν_3	1582	1603	1594	1615	1613
ν_4	1374	1375	1371	1391	1389
ν_5	1204	1203	1192	1196	1195
ν_6	994	980	974	978	976
ν_7	754	734	726	725	724
ν_8	613	616	616	613	612
ν_9	333	341	338	337	336

(a) From ref. (11).

(b) From ref. (10).

(c) From ref. (21).

Table 5. Calculated and experimental frequencies (cm^{-1}) of A_g modes of $TCNQ^{=}$.

Mode	$TCNQ^{=}$ calc.	$TCNQ^{=}$ (soln)[a]	Na_2TCNQ[b]
ν_2	2196	2119	2150
ν_3	1570	1615	1597
ν_4	1316	1311	1328
ν_5	1204	1191	1194
ν_6	1024	-	999
ν_7	781	739	731
ν_8	623	-	624
ν_9	333	-	-

(a) From ref. (38).

(b) From ref. (11).

Table 6. Calculated bond orders, bond self-polarizabilities and force constants for $TCNQ^{-0.59}$.

Bond	1-2	1-5	5-7	7-9	9-13
P_r	0.82196	0.43241	0.68639	0.31571	0.93129
$\pi_{r,r}$ ($10^{10}erg^{-1}$)	-2.1483	-4.9540	-3.6675	-5.2225	-0.9386
K_r (10^5dyn/cm)	9.925	7.766	9.164	7.117	17.952

Table 7. Bond order and bond length changes for $TCNQ^-$ due to $^2B_{2g} \rightarrow {}^2B_{1u}^{(1)}$ electronic transition

Bond	ΔP_r	$\Delta r(A^\circ)$
1-2	-0.12446	+0.0219
1-5	+0.11630	-0.0205
5-7	-0.22020	+0.0388
7-9	+0.02838	-0.0050
9-13	-0.01186	+0.0021

Figure Captions

Figure 1. Electronic absorption spectra of CuTCNQ (a) CH_3CN solution, (b) thin film on SiO_2 and (c) nujol mull.

Figure 2. Electronic absorption spectra of TCNQ, (a) CH_3CN solution and (b) nujol mull.

Figure 3. Raman spectra of CuTCNQ salt.

Figure 4. Raman spectra of TCNQ, powder in a capillary tube.

Figure 5. Raman spectra of thin CuTCNQ film, prepared on aluminum substrate.

Figure 6. Numbering scheme and internal symmetry coordinate definitions.

Figure 7. Calculated frequencies of ν_4 mode as a function of charge transfer ρ.

Figure 8. Resonance Raman spectra of AgTCNQ and LiTCNQ. AgTCNQ is in the form of film ($\sim$ 5 μm) prepared by dipping a clean Ag foil into hot CH_3CN solution of TCNQ (16). LiTCNQ was prepared by the reaction of LiI and TCNQ (16), and is in the form of a KBr pellet.

Figure 9. Molecular geometries of $TCNQ^-$ in the ground, (——) $^2B_{2g}$, and excited (---), $^2B_{1u}$ (1), electronic state. Arrows represent atomic displacements during the electronic excitation.

Figure 10. Calculated and observed resonance Raman spectrum of $TCNQ^-$ in the red-band system. The values of the frequencies of the calculated spectrum are also the calculated ones.

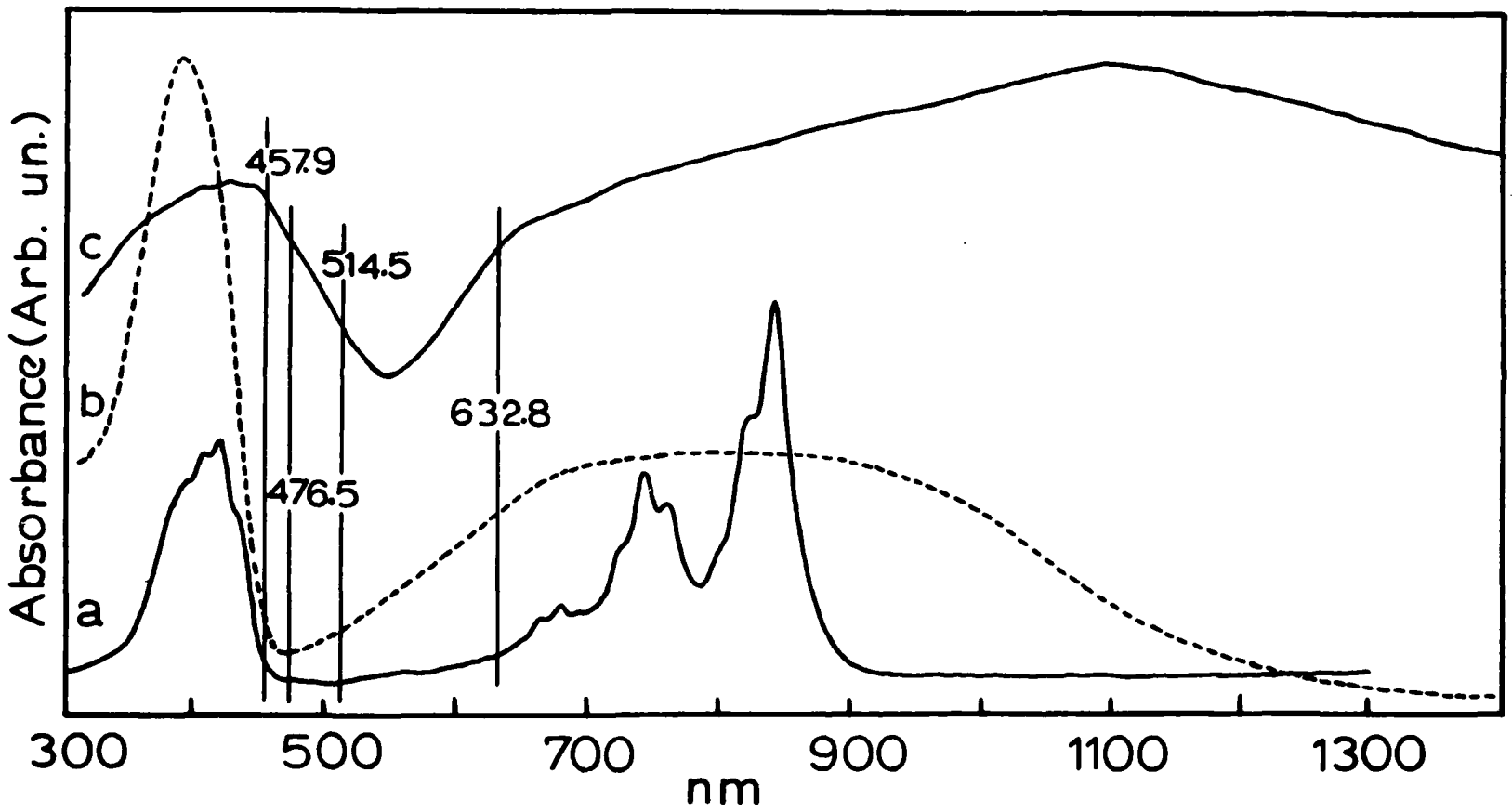
Absorbance (Arb. un.)
c
b
a
457.9
514.5
476.5
632.8
300
500
700
900
1100
1300
nm

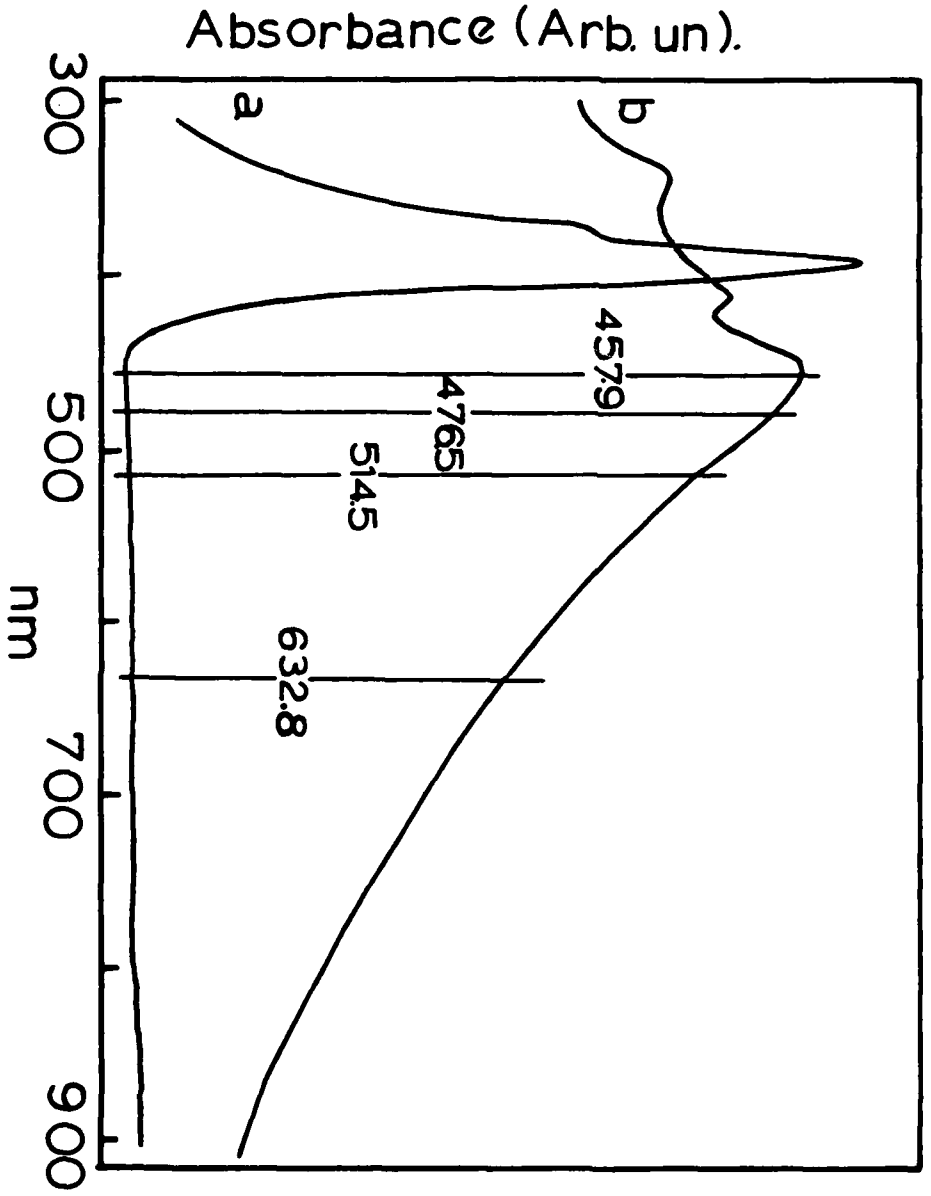
Absorbance (Arb. un).
300
500
700
900
nm
a
b
457.9
476.5
514.5
632.8

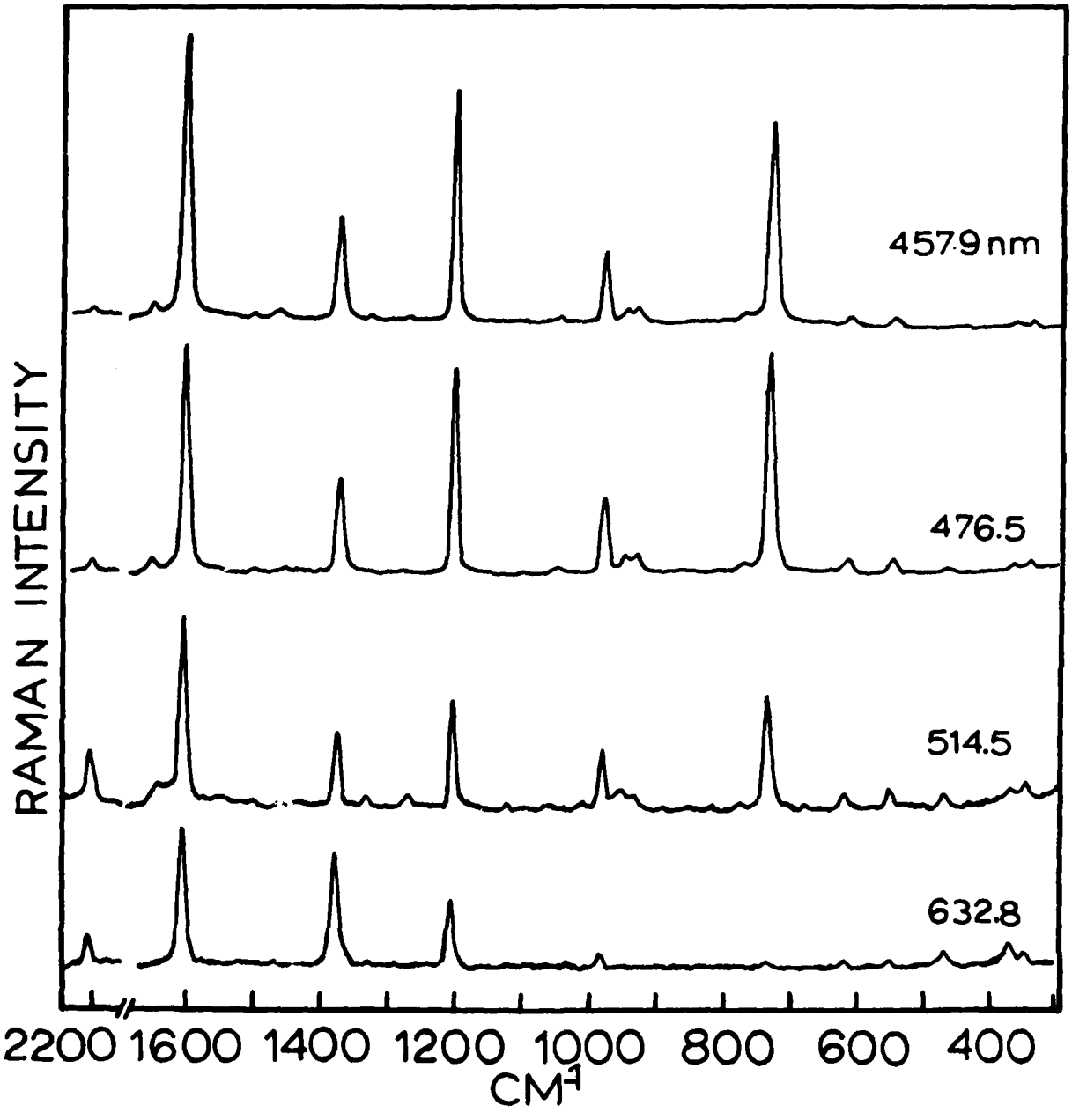
457.9 nm
476.5
514.5
632.8
RAMAN INTENSITY
2200 1600 1400 1200 1000 800 600 400
CM-1

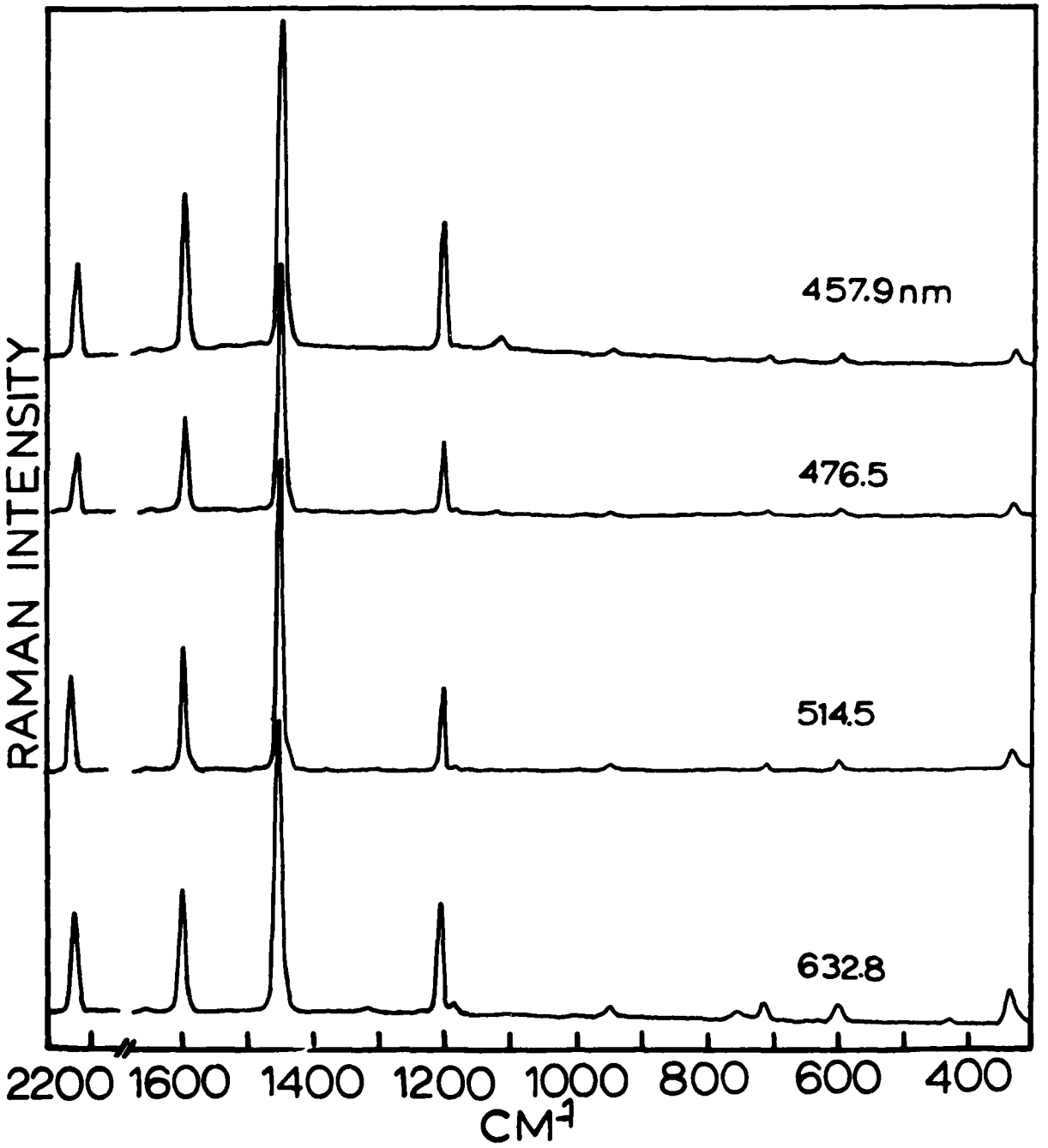
RAMAN INTENSITY
457.9nm
476.5
514.5
632.8
2200 1600 1400 1200 1000 800 600 400
CM-1

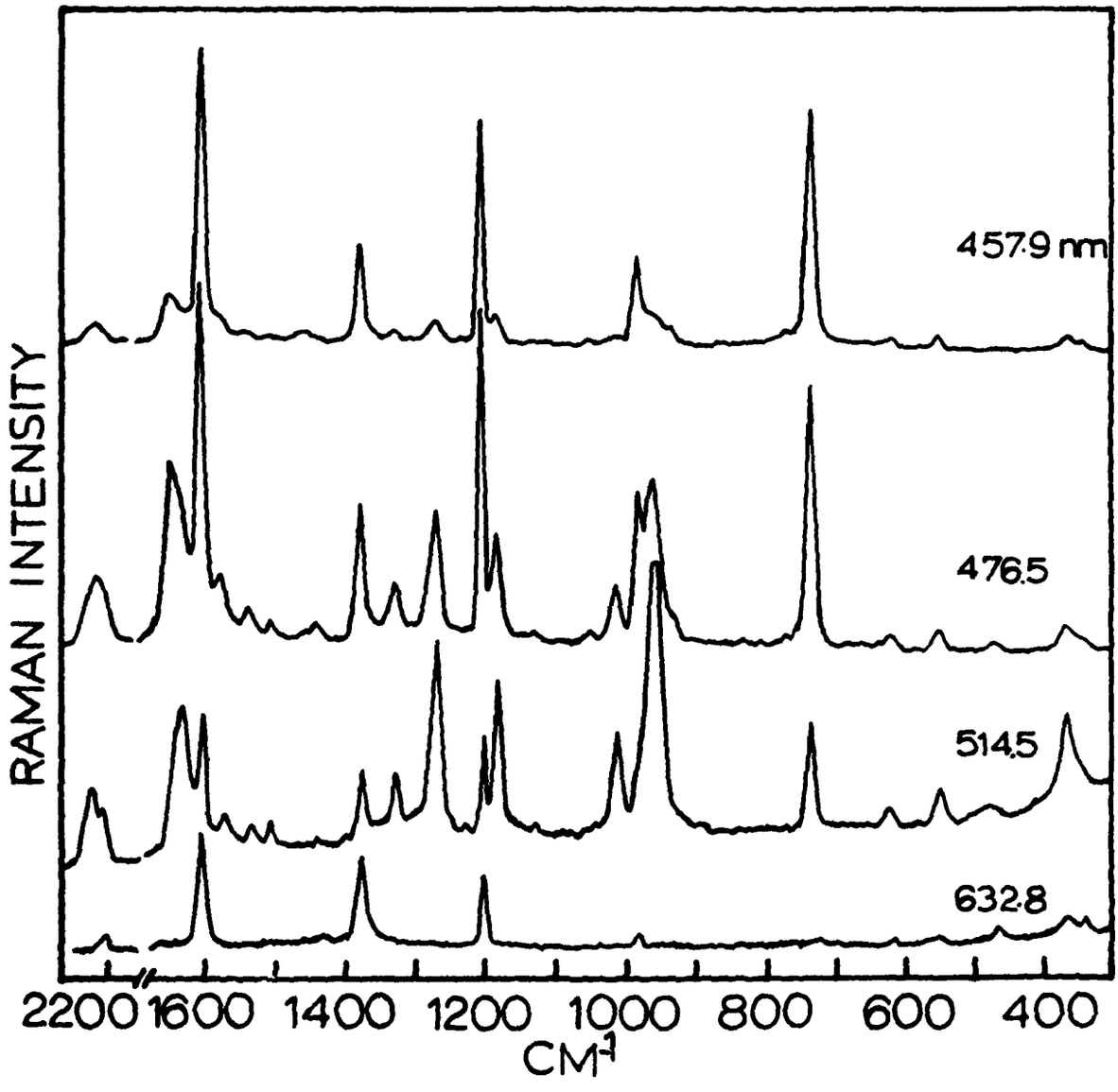
RAMAN INTENSITY
457.9 nm
476.5
514.5
632.8
2200 1600 1400 1200 1000 800 600 400
CM-1

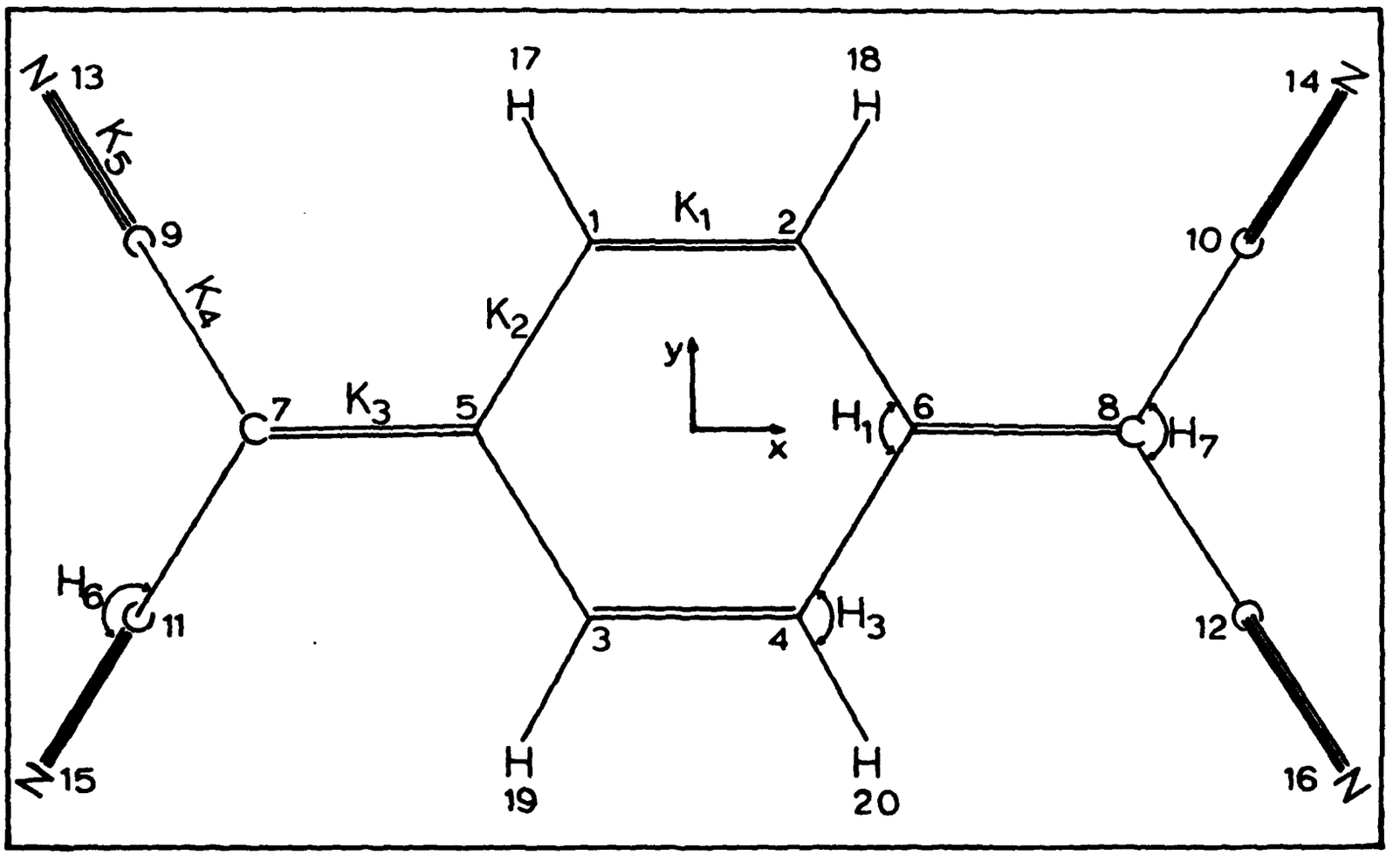
N 13
K5
9
K4
17
H
18
H
14 N
1
K1
2
10
K2
y
x
7
K3
5
H1
6
8
H7
H6
11
3
4
H3
12
N 15
H
19
H
20
16 N

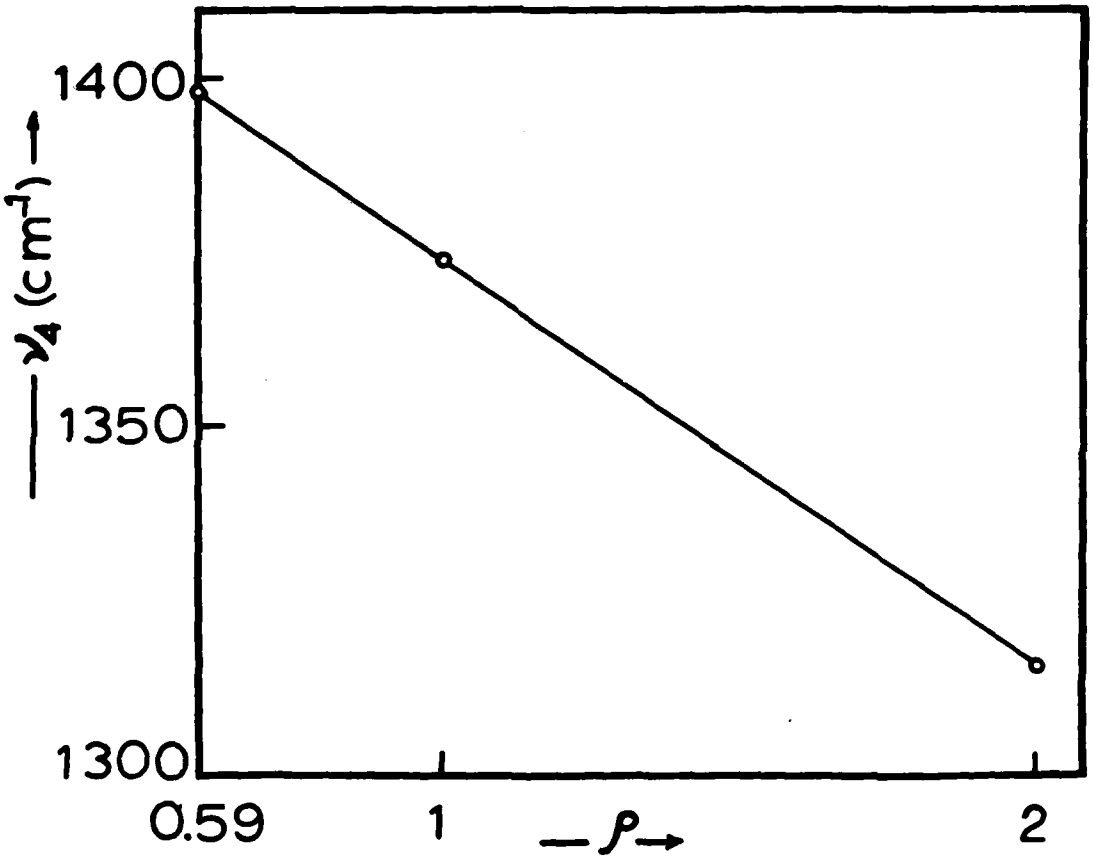
1400
1350
1300
ν_4 (cm^{-1})
0.59
1
2
ρ

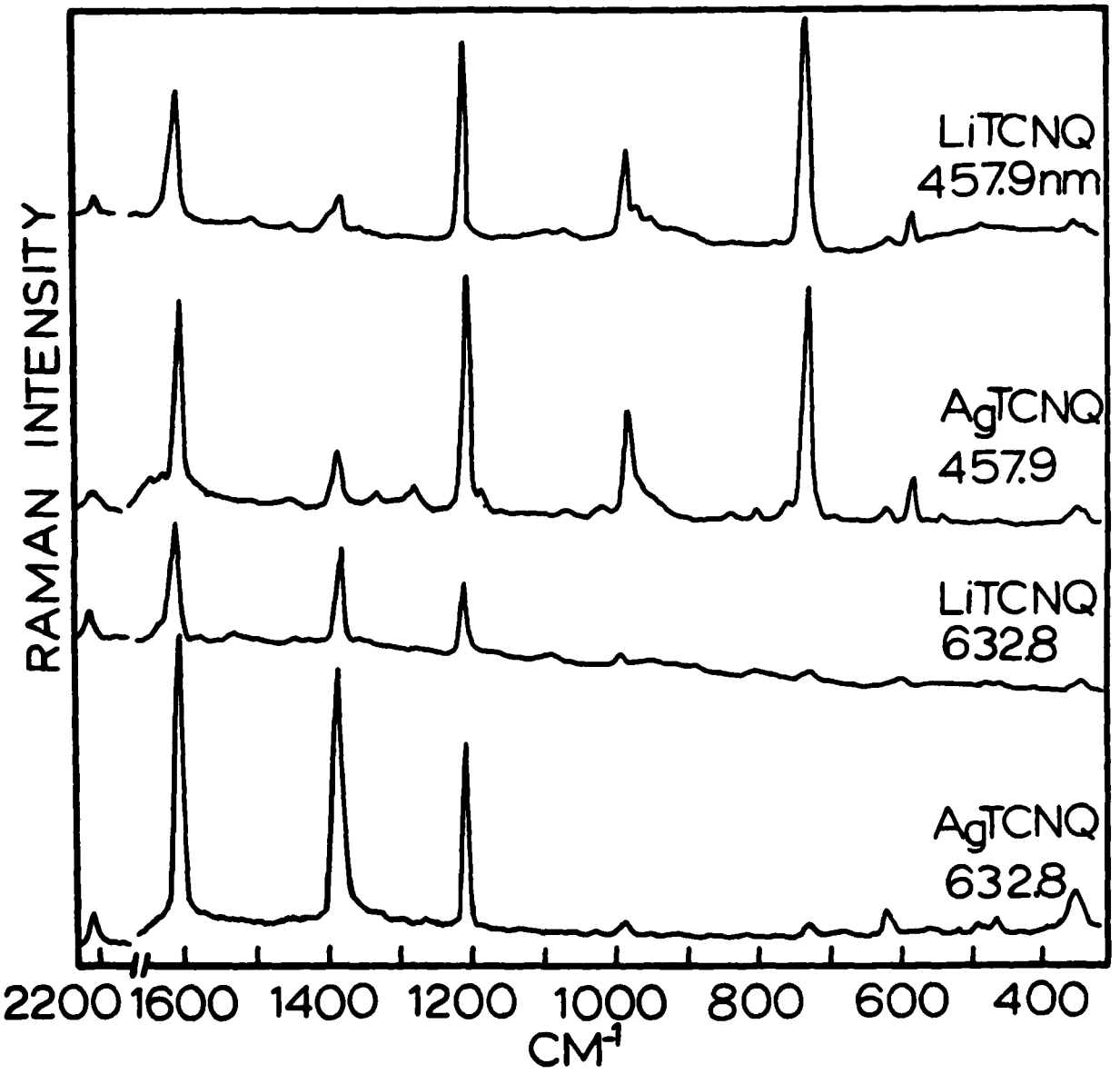
LiTCNQ
457.9nm
AgTCNQ
457.9
LiTCNQ
632.8
AgTCNQ
632.8
RAMAN INTENSITY
2200 1600 1400 1200 1000 800 600 400
CM-1

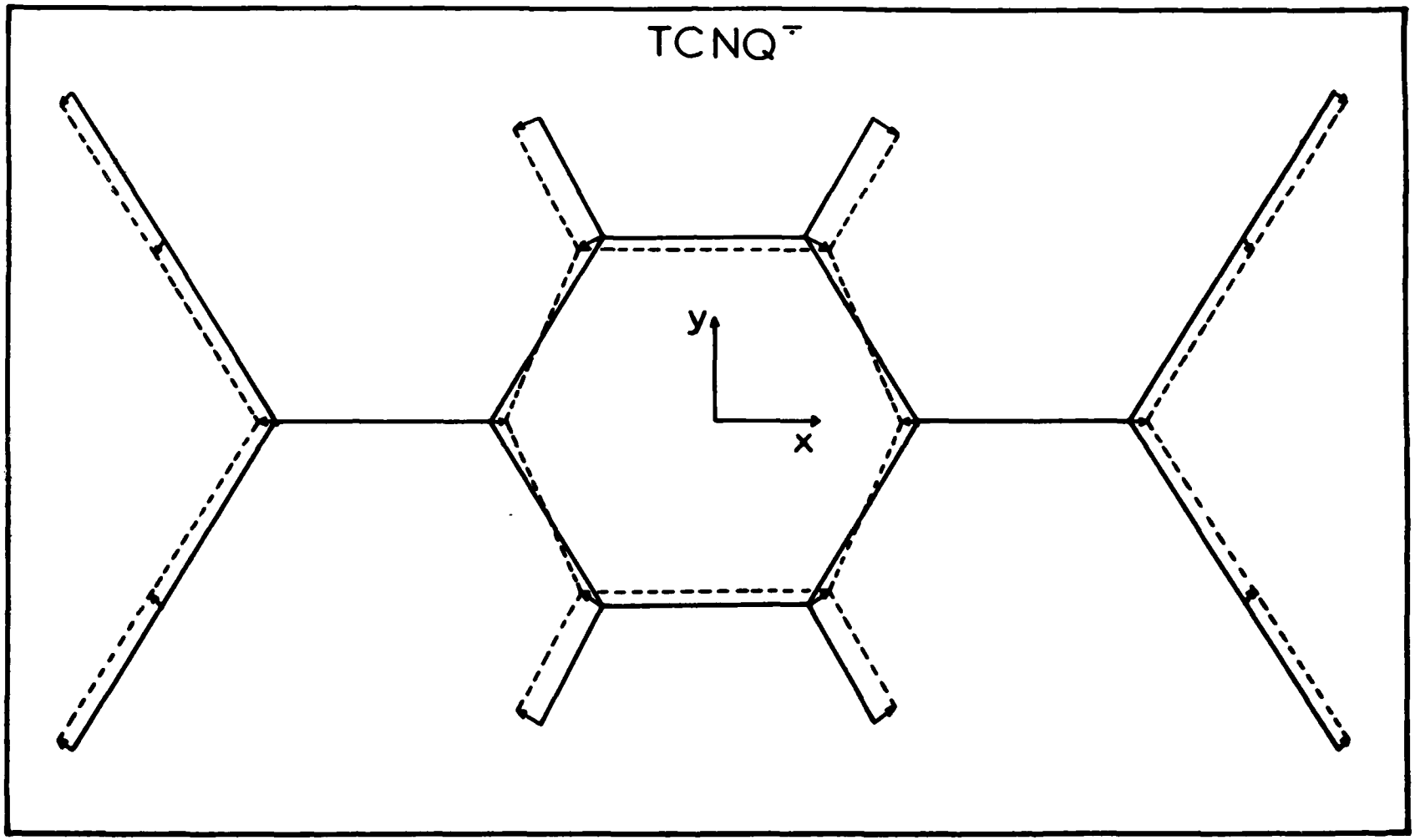
TCNQ⁻
y
x

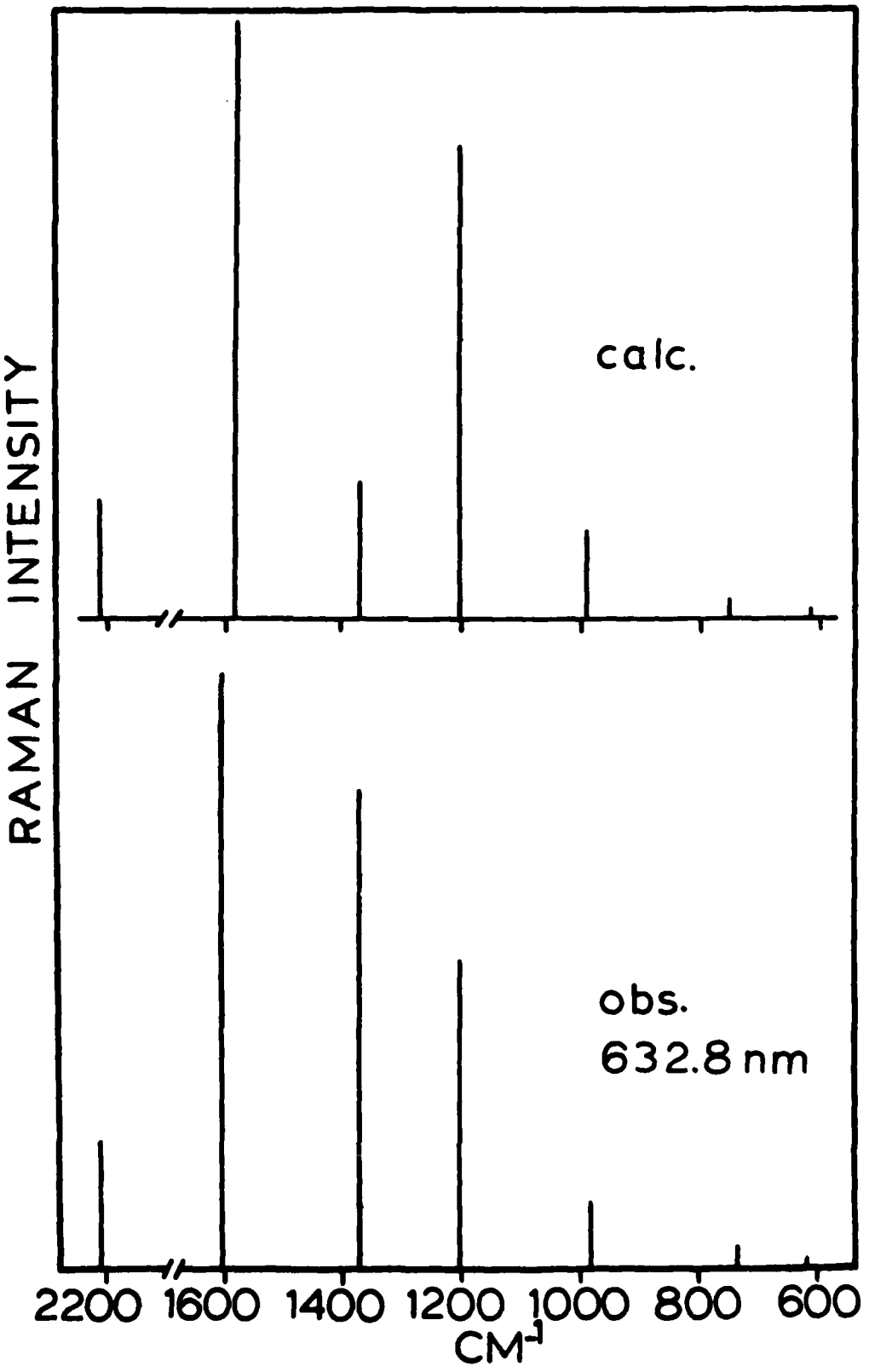
RAMAN INTENSITY
calc.
obs.
632.8 nm
2200 1600 1400 1200 1000 800 600
CM-1


ATE
LME